Available online at www.sciencedirect.com
SCIENCE DIRECT
Journal of Power Sources 157 (2006) 537–542
JOURNAL OF POWER SOURCES
www.elsevier.com/locate/jpowsour

Differential voltage analyses of high-power lithium-ion cells 3. Another anode phenomenon

Ira Bloom [a,*], Jon P. Christophersen [b], Daniel P. Abraham [a], Kevin L. Gering [b]

[a] *Electrochemical Technology Program, Argonne National Laboratory, 9700 South Cass Avenue, Argonne, IL 60439, USA*
[b] *Idaho National Laboratory, P.O. Box 1625, Idaho Falls, ID 83415, USA*

Received 15 June 2005; received in revised form 28 July 2005; accepted 29 July 2005
Available online 2 November 2005

Abstract

We characterized high-power lithium-ion cells in terms of performance and cycle and calendar life at 45 °C. Among other parameters, we measured the *C*/25 capacity every 4 weeks during the test. Differentiation of the *C*/25 voltage versus capacity data with respect to capacity (d*V*/d*Q*) has been used to elucidate another type of side reaction at the anode. In cycle-life cells, with their higher capacity throughput, the analysis showed that one phase transition (a peak in the profile) was disappearing with time. In contrast, this effect was not seen in calendar-life cells.
© 2005 Elsevier B.V. All rights reserved.

Keywords: Battery; Differential voltage analysis; Lithium-ion; Aging

1. Introduction

Lithium-ion batteries represent the state-of-the art where a high specific- or volumetric-energy or power-density battery is required. These batteries usually consist of a lithiated transition metal oxide positive (cathode), a lithiated carbonaceous negative (anode), and a lithium salt dissolved in an organic solvent (electrolyte). High-power lithium-ion batteries are being considered for use in automotive applications by the U.S. Department of Energy (DOE)-supported Freedom Cooperative Automotive Research Partnership. The DOE established the Advanced Technology Development Program to help battery developers overcome key barriers to the automotive application. Among these are life, safety, cost, and low-temperature operation.

Two national laboratories, Argonne National Laboratory (ANL) and Idaho National Laboratory (INL), collaborated to understand some of the life-limiting phenomena: the causes of resistance rise and capacity and power fade in lithium-ion batteries [1]. This work showed that the *C*/25 capacity data and the beginning-of-life cell resistance and power data were well correlated with a square-root-of-time ($t^{1/2}$) dependence. This common dependence on $t^{1/2}$ suggests that one or more degradation mechanisms are affecting all cell performance parameters in a like manner.

Some of the *C*/25 data were presented in earlier papers [2,3] to describe and demonstrate the use of differential voltage (d*V*/d*Q*) curves to elucidate some of the locations and types of fade mechanisms in lithium-ion batteries. The d*V*/d*Q* curves permitted easy graphical analysis, whereas using differential capacity curves (d*Q*/d*V*) was more problematic. Phenominologically speaking, the peaks in the d*V*/d*Q* curves are from phase transitions, whereas the peaks in the d*Q*/d*V* curves are from pseudo-phase equilibria (i.e., very small polarization). Under these conditions, d*V* = 0 and the value of d*Q*/d*V* is undefined. On the other hand, with a constant current discharge (or charge) to generate the data, d*Q* is always nonzero.

The peaks in the d*V*/d*Q* curves were assigned to cathode, anode, or their sum by comparison to half-cell data. The earlier papers showed how to apply the d*V*/d*Q* techniques to understand two cases. In the first, we showed that the capacity fade could be primarily due to side reactions at the anode. In the second, we showed how to use d*V*/d*Q* curves in a

* Corresponding author. Tel.: +1 630 252 4516; fax: +1 630 972 4516.
E-mail address: bloom@cmt.anl.gov (I. Bloom).

0378-7753/$ – see front matter © 2005 Elsevier B.V. All rights reserved.
doi:10.1016/j.jpowsour.2005.07.054

more complicated case in which there was evidence of complex physical as well as chemical phenomena occurring at the anode. These phenomena were observed in both the calendar- and cycle-life experiments.

In the work that follows, we continue the discussion, focusing on the aging of the anode. We show that, by using dV/dQ curves to analyze cell data, other, more subtle changes at the anode can be visualized. These changes were seen in all cycle-life cells, but were most noticeable in four of them.

2. Experimental

2.1. 18650-Sized cells

Detailed information regarding cell construction is given in Reference [1], and the testing regime is given in References [1,4,5]. The cell chemistry is given in Table 1. The average active area was 846.3 cm^2, and the nominal C/1 capacity was 0.8 Ah. The four cells that are discussed below came from a population of 26 weld-sealed, 18650-sized cells. These cells were fabricated to ANL's specifications for this work. The cells underwent formation cycles before delivery. Fifteen of the 26 cells were delivered to INL, and 11 were delivered to ANL. After characterization at 25 °C, one cell was removed from testing at both sites. This left 14 cells at INL for cycle-life testing at 45 °C and 10 cells at ANL for calendar-life testing at 45 °C (see References [4,5] for more information regarding the test procedures and the test plan).

The test procedures are defined in References [4,5]. Briefly, the calendar test consisted of potentiostating the cells at 60% SOC (3.741 V) at 25 °C, heating the cells to the test temperature, and, while remaining at the test temperature, performing the profile shown in Fig. 1 once per day. The cycle-life test consisted of using the profile given in Fig. 2 at 60% SOC at the test temperature.

The cells were characterized in terms of their charge and discharge C/25 (0.032-A rate) capacities before the tests began. After 4 weeks (or 33,600 cycles) at temperature, the cells were cooled to 25 °C and reference performance tests (RPTs) were performed. The RPTs consisted of portions of the characterization tests, including the C/25 tests. The cells were then heated back to the test temperature. The process was repeated until the power fade at the 300-Wh line was greater than 50%. The test types differed in the amount of lithium capacity charged and discharged during a 4-week period. For the calendar-life cells, it was about 7 Ah, and about 735 Ah for the cycle-life cells.

Table 1
Cell chemistry

Cathode electrode	Anode electrode
8 wt.% PVDF binder (Kureha KF-1100)	8 wt.% PVDF binder (Kureha #C)
4 wt.% SFG-6 graphite (Timical)	92 wt.% MAG-10 (Hitachi)
4 wt.% carbon black (Chevron)	
84 wt.% $LiNi_{0.8}Co_{0.1}Al_{0.1}O_2$	4.9 mg/cm^2 loading density
8 mg/cm^2 loading density	35-μm-thick coating/side
35-μm-thick coating/side	18-μm-thick Cu current collector
30-μm-thick Al current collector	
Electrolyte	**Separator**
1.2 M $LiPF_6$ in EC/EMC (3:7, w/w)	25-μm-thick Celgard 2325 separator

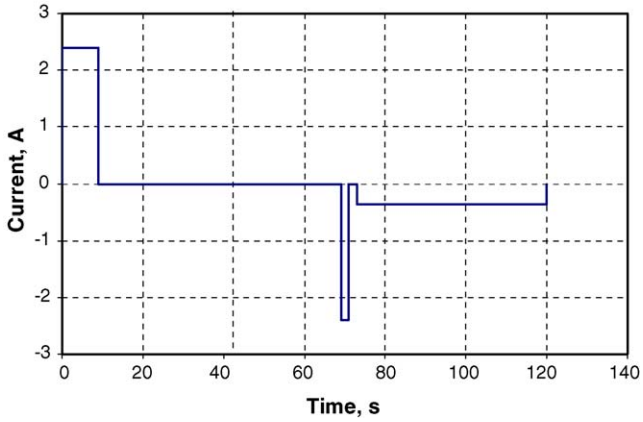

Fig. 1. Calendar-life test pulse profile. This profile was performed once per day. Positive current is discharge.

2.2. Half-cells

Half-cell construction from fresh and aged 18650 materials was described in prior papers [2,3]. The half-cells were charged and discharged at the C/25 rate. The charge and discharge voltages were measured and recorded every 30 s. This yielded about 2500–4800 data points for analyses.

2.3. Data reduction and calculations

As described earlier [2,3], the C/25 charge and discharge data from the cells from each test population, as

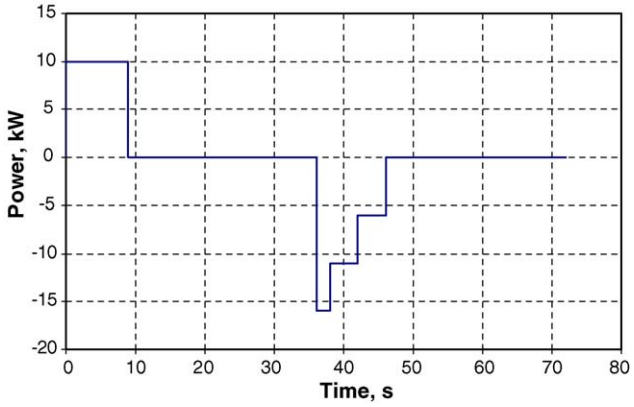

Fig. 2. 25-Wh profile used in cycle-life tests. The profile was scaled down by a factor of 651. Positive current is discharge.

well as from the half-cells, were noisy due to the very slow charge/discharge rates. Mathematical filtering was used to average out the noise and accentuate the peaks. The filtering was performed using Microsoft Excel, and consisted of calculating the percent depth-of-discharge (%DOD) for each point based on the experimental data and then using the FORECAST function to interpolate the cell capacity and voltage at evenly spaced %DOD intervals. Typically, 0.5%DOD intervals were used, yielding 200 points for subsequent manipulation and plotting. $-Q_o\,dV/dQ$ was calculated as $-Q_o \times \Delta V/\Delta(\text{Ah})$, where Q_o is the measured $C/25$ capacity of the cells (in Ah), $\Delta(\text{Ah})$ the change in the capacity of the cell in a given interval, and ΔV is the change in cell voltage as a result of $\Delta(\text{Ah})$. The Q_o factor served to normalize the derivatives based on cell capacity. Further smoothing of $-Q_o\,dV/dQ$ was accomplished by using a 5-point moving average. Plots of $-Q_o\,dV/dQ$ versus capacity density (mAh/cm^2) were then analyzed for trends.

In the half-cell work, the full-cell potential was calculated by subtracting the anode potential from that of the cathode. Similarly, the full-cell derivatives were calculated as the differences between the potentials of the cathode and the anode. However, the calculated derivates were different from the observed. Better agreement between calculated and observed was obtained by allowing misalignment in the working capacity/potential windows of the electrodes. In an earlier work, this misalignment was termed as "slippage" [2]. For the electrode-slippage calculation, the electrode alignments relative to each other were shifted from left to right depending on which section of the total electrode capacity was actually used in the cell. The cell capacity was defined as being between the voltage limits of 4.1 and 3.0 V.

Before comparing the 18650- and half-cell data, the 18650-cell data were shifted relative to the data from the anode half cell. The active area was also decreased. This aligned the voltage versus capacity discharge curves of the two types of cells. Once the adjustments were made, they were not changed.

3. Results

The initial $C/25$ discharge curve is given in Fig. 3a and is typical for these lithium-ion batteries. Differentiating these data with respect to capacity yields the plot shown in Fig. 3b. Using the principles described earlier [2,3], the cathode and anode discharge curves were realigned by shifting the cathode relative to the anode. The operating voltage window of 3–4.1 V was kept constant. The results of these calculations are given in Fig. 3c, which shows the contributions from the electrodes to the five peaks in Fig. 3b. Fig. 3c shows that peak 1 is from the cathode, that peak 2 is from the sum of cathode and anode, and that peaks 3–5 are from the anode. From the figure, one can see that the curves from half-cell data and from the actual 18650 cell agree well.

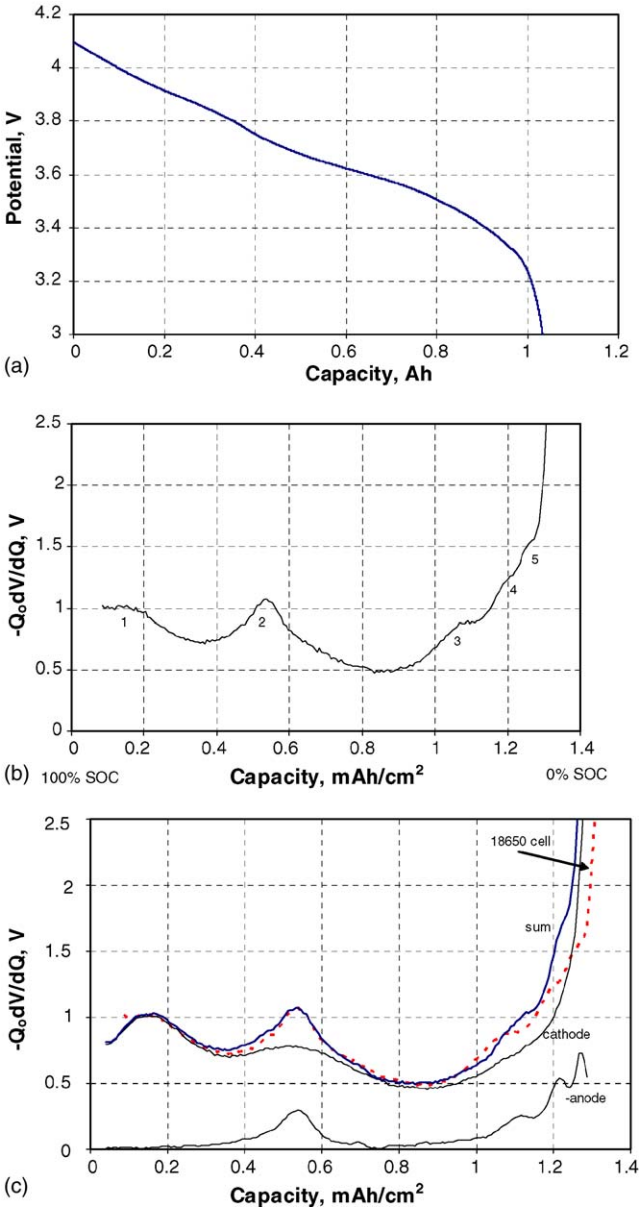

Fig. 3. (a) Plot of potential vs. capacity for a lithium-ion cell at $t = 0$ weeks and at 25 °C. The initial (0.032-A rate) $C/25$ capacity for this cell was 1.03 Ah. (b) Plot of $-Q_o\,dV/dQ$ vs. capacity using the data in Fig. 1a. The SOC convention used in this figure is implicit in the other plots of dV/dQ that follow. (c) $-Q_o\,dV/dQ$ vs. capacity curves calculated from cathode and anode half-cell data, their sum, and from 18650 data. For the half-cell calculation, the cathode data were shifted by 0.27 mAh/cm^2 relative to the anode.

As the cell ages, the capacity fades. The change in $C/25$ capacity is reflected by changes in the dV/dQ curves, which are shown for two cells, cells 1 and 2, in Fig. 4a and b, respectively. Cell 1 was cycled for 92 weeks, and cell 2 was cycled for 72 weeks. In these figures, the peak pattern shifts to the left with capacity fade. Additionally, the peak labeled 2 in Fig. 3b separates into its constituents. Peak 2′ in Fig. 4a and b emerges from beneath peak 2 as the cell ages. Further, Fig. 4a and b shows that the positions of peaks 1 and 2′ do not change with time. Yet, peaks 2–5 shift to the left as capacity is lost.

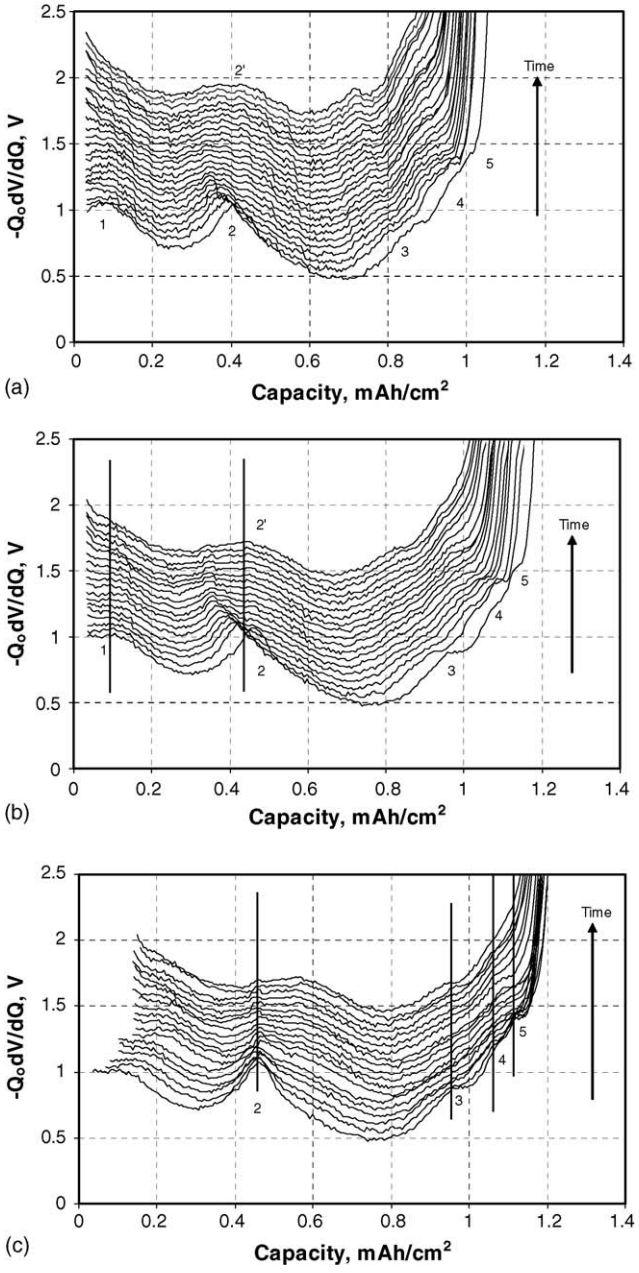

Fig. 4. (a) Changes in the plot of $-Q_o\,dV/dQ$ vs. capacity with time for cycle-life cell 1. A vertical offset was added to the curves for the sake of clarity. The total *C*/25 capacity loss after 96 weeks was 11.6%. (b) Changes in the plot of $-Q_o\,dV/dQ$ vs. capacity with time for cycle-life cell 2. A vertical offset was added to the curves for the sake of clarity. Peaks 1 and 2′ do not move with time. The total *C*/25 capacity fade after 72 weeks was 10.9%. (c) Data shown in (b) with the curves replotted so that peak 2 is aligned.

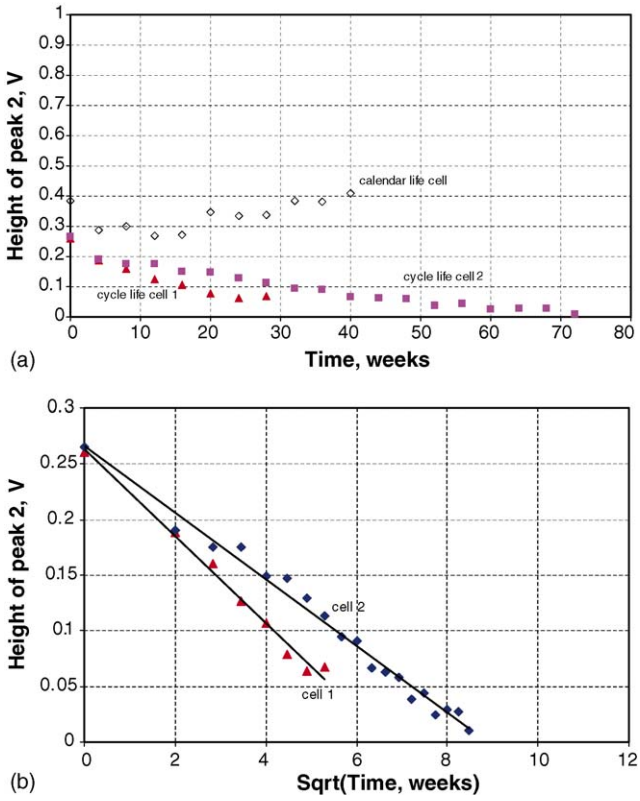

Fig. 5. (a) Height of peak 2 as a function of time for a calendar-life cell and two cycle-life cells. Peak 2′ and the background were subtracted before plotting. (b) Height of peak 2 vs. the square root of time for two cycle-life cells. Peak 2′ and the background were subtracted before plotting. The height of peak 2 in cell 1 was not resolvable from the background after 44 weeks of aging. The value of the regression coefficient, r^2, in both cases was 0.99.

Replotting the data in Fig. 4b with peak 2 aligned (Fig. 4c) shows that peaks 2–5 are related. Based on half-cell results, these peaks are from the anode. Peaks 1 and 2′ are from the cathode. Using the principles discussed in References [2,3], the shifting is most likely due to lithium-consuming side reactions at the anode. Detailed discussions on the interpretation of the peak shifts are given in References [2,3] and will not be discussed further here.

From an inspection of Fig. 4a and b, only peak 2 is sufficiently resolved for further analysis. Peak 1 (cathode) is well resolved at the beginning of life, but tends to broaden as the cell ages. Peak 2′ (also cathode) is the reverse; it is poorly resolved at the beginning of life and tends to become resolved with time. Peaks 3–5 (anode) are not well defined throughout the experiment. In principle, d*V*/d*Q* analysis could provide information on other processes, such as those at the cathode, using these peaks, but cannot with the examples given in Fig. 4a and b.

In the figures, the intensity of peak 2 of the cycle-life cells decreases as the cells age. This is shown in Fig. 5a. Also given in Fig. 5a is a plot of the intensity of peak 2 over time from a typical calendar-life cell. The peak heights from the calendar-life cell appear to be constant within experimental error. This is in sharp contrast to that seen for the cycle-life cells. The difference is most likely due to the amount of lithium exchanged. In the calendar-life test, the amount of lithium exchanged during charge and discharge during the test was about 7 Ah per 4-week period; in the cycle-life test, it was about 735 Ah per 4-week period.

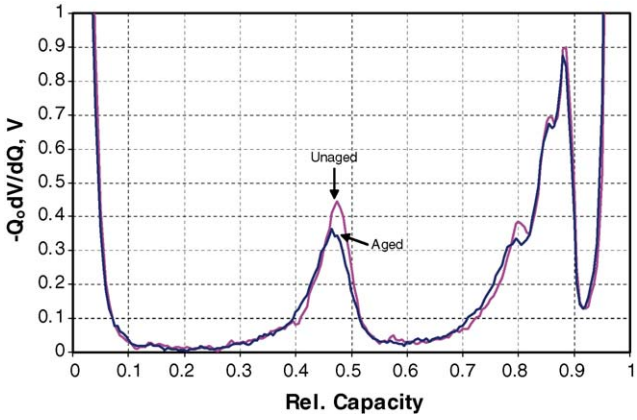

Fig. 6. Plots of $-Q_o\,dV/dQ$ vs. relative capacity from half-cells containing aged and unaged anode materials. The aged material is from cell 2.

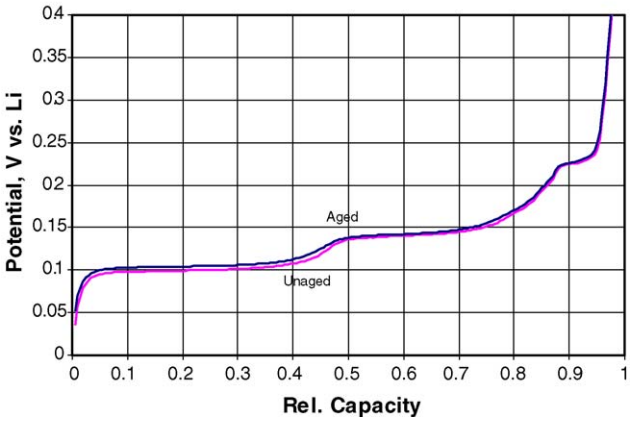

Fig. 7. Half-cell potentials (vs. Li) of aged and unaged anode materials vs. relative capacity from cell 2. The data were obtained at the *C*/25 rate. The capacity scale has been normalized to eliminate differences in half-cell capacity.

Plotting the height of peak 2 data from the two cycle-life cells shows that the height depends inversely on $t^{1/2}$ and the rate at which the intensity of peak 2 decreases is faster for cell 1 than for cell 2. The plots of the height data versus the square root of time are shown in Fig. 5b. Linear regression fits of the data in Fig. 5b have regression coefficients, r^2, equal to 0.99. From the slopes of these lines, the respective rate constants are 3.91×10^{-2} V/week (S.E. = 0.17×10^{-2}) and 3.00×10^{-2} V/week (0.09×10^{-2}) for cells 1 and 2, respectively.

Given the above observations, the question now is whether the behavior is due to cell construction [3] or is partly due to the anode material. A portion of the aged anode material was characterized by *C*/25 capacity measurement in a half-cell. To remove the effect of the difference in half-cell capacities, the d*V*/d*Q* versus capacity curves from the aged anode material and that from unaged anode material were normalized to the height of the low-SOC anode peak. These curves are plotted versus relative or fractional capacity in Fig. 6. This aligned peaks 3–5 and highlighted the differences in peak 2. From the figure, the height of peak 2 changes with aging. Thus, the effect observed in the 18650 (Fig. 4a) is reproducible in a half-cell (Fig. 6), indicating that some of the changes caused by cycling are partly due to the anode material.

Further analysis of the *C*/25 data reveals more clues as to the source of the decrease in height of peak 2. Fig. 7 shows the *C*/25 voltage discharge profiles versus relative capacity for the unaged and aged anode material. The figure shows that there are differences between the two curves. Comparing the voltages of the plateaus in the relative capacity range of 0.2–0.3 shows that there is a 5-mV increase in the plateau from the aged anode. The voltage of the next plateau (relative capacity range of 0.55–0.7) has not changed appreciably. Thus, the change in voltage associated with the phase transition has decreased. Since d*Q* was constant in the experiments, the decrease in voltage change (d*V*) caused the height of peak 2 to decrease. Conceptually, the difference in lithium activity between the two phases in the anode has decreased. In Fig. 4a and b, the lithium activity difference approached zero.

4. Discussion

In an earlier paper [1], we categorized capacity loss as due to two main mechanisms. The first, loss of accessible material, capacity of an electrode is uniformly lost. The second is where there is a shift in the alignment of the electrodes due to side reactions. These side reactions consume lithium capacity, but do not change the actual capacity of the electrode. An example of these side reactions is the formation of the solid electrolyte interphase layer. This concept, called "slippage" above, was used to initially align the half-cell data so that they better represent the data from the 18650 cells. These mechanisms have different effects on the behavior of the d*V*/d*Q* curve. In the first case, the loss of accessible material causes distances between peaks to decreases; hence, the peaks from the same electrode move together with time. In the second case, the side reactions cause peaks to appear and disappear at different ends of the d*V*/d*Q* versus SOC curve. Based on our earlier results [1], side reactions were the most likely cause of capacity fade in these cells.

As mentioned in Section 3, the most likely cause of *C*/25 capacity loss is by side reactions at the anode. The above results outline one of many undesirable side reactions. Here, the electrochemically active layers within the carbon anode particles are reacting with solvated lithium ions in such a way that the products of the reaction remain in the "galleries" between the graphene layers. This is shown schematically in Fig. 8. The effects of solvent co-intercalation and reactions on the physical properties of various graphites have been reported in the literature [6–13]. For example, Besenhard et al. studied the film-forming reactions of graphite materials in organic electrolytes [7,11]. They found that there was an initial irreversible reaction that led to a complex film from the chemical decomposition of solvated graphite-intercalation compounds, $Li(solv)_yC_x$, where "solv" is a mixture of solvent molecules. Further, Besenhard states that, since the

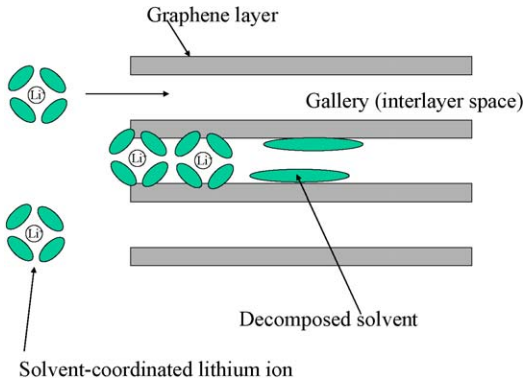

Fig. 8. Schematic showing solvent-coordinated lithium ions entering galleries between graphene layers. Some decomposed solvent remains in interlayer space.

unsolvated Li^+ ion is small, it can still participate in the reversible intercalation process even if the space between the graphene layers is filled with organic decomposition products [11]. Thus, one would expect that the cell would continue to operate as the space between the layers fills. The filling of the interlayer space with lithiated organic materials is the most likely source of the decrease in lithium activity difference between the two phases. Indeed, filling of the galleries has been reported by Peled et al. [12].

The difference in relative rates of filling between the calendar- and cycle-life cells can be traced to the capacity throughput. Based on the way the experiments were performed, the cycle-life cells experienced more than 105 times the capacity throughput per month of the calendar-life cells. With the increase in throughput, more coordinated organic solvent molecules are present, increasing the likelihood of a decomposition reaction.

The data in Fig. 5a correlate well with $t^{1/2}$, indicating that the underlying mechanism is most likely diffusion controlled. During the early stages, 0–4 weeks, the rate of reaction is relatively fast, since the interlayer space is empty of organic material. As the space fills during subsequent weeks, the rate slows down. Thus, the height of peak 2 is an indicator of the amount of lithiated organic material remaining in the galleries.

5. Conclusions

dV/dQ analysis of C/25 capacity data has been used to elucidate another type of side reaction at the anode. In cycle-life cells, with their higher capacity throughput, the analysis showed that one phase transition (a peak in the profile) was disappearing with time. In contrast, this effect was not seen in calendar-life cells.

In situations where using a reference electrode is not practical or possible, much information can be gained from the C/25 capacity data from aging cells. The above discussion illustrates the use of dV/dQ analysis to delineate an undesirable side reaction at the anode in sealed operating cells.

Acknowledgments

This work was performed under the auspices of the U.S. Department of Energy, Energy Efficiency and Renewable Energy, Office of FreedomCAR and Vehicle Technologies, under Contract Nos. W-31-109-Eng-38 (ANL) and DE-AC07-05ID14517 (INL).

References

[1] I. Boom, S.A. Jones, V.S. Battaglia, G.L. Henriksen, J.P. Christophersen, R.B. Wright, C.D. Ho, J.R. Belt, C.G. Motloch, J. Power Sources 124 (2003) 538.
[2] I. Bloom, A.N. Jansen, D.P. Abraham, J. Knuth, S.A. Jones, V.S. Battaglia, G.L. Henriksen, J. Power Sources 139 (2005) 295.
[3] I. Bloom, J. Christophersen, K. Gering, J. Power Sources 139 (2005) 304.
[4] PNGV Battery Test Manual, DOE/ID-10597, Rev. 3, February 2001.
[5] PNGV Test Plan for Advanced Technology Development Gen 2 Lithium-Ion Cells, EHV-TP-121, Rev. 6, October 5, 2001.
[6] R. Fong, U. von Sacken, J.R. Dahn, J. Electrochem. Soc. 137 (1990) 2009.
[7] J.O. Besenhard, M. Winter, J. Yang, W. Biberacher, J. Power Sources 54 (1995) 228.
[8] M. Inaba, Z. Siroma, Y. Kawatate, A. Funabiki, Z. Ogumi, J. Power Sources 68 (1997) 221.
[9] M. Inaba, Z. Siroma, A. Funabiki, Z. Ogumi, Langmuir 12 (1996) 1535.
[10] M. Winter, J.O. Besenhard, M.E. Spahr, P. Novák, Adv. Mater. 10 (1998) 725.
[11] J.O. Besenhard, Carbon 14 (1976) 111.
[12] E. Peled, D. Bar Tow, A. Merson, A. Gladkich, L. Burstein, D. Golodnitsky, J. Power Sources 97–98 (2001) 52.
[13] R. Yazami, Y.F. Reynier, Electrochim. Acta 47 (2002) 1217.